Failure Analysis of Two HP-Nb Heat-Resistant Tubes after 46,000 h Exposure to Reformer Service Conditions

Harandi , Ali Nazemi ; Eslami, Abdoulmajid ; Bahrami, Abbas; Bakhtafrouz, Asghar ; Yazdan Mehr, Maryam

DOI
10.3390/met13020228

Publication date
2023

Document Version
Final published version

Published in
Metals

Citation (APA)
Harandi , A. N., Eslami, A., Bahrami, A., Bakhtafrouz, A., & Yazdan Mehr, M. (2023). Failure Analysis of Two HP-Nb Heat-Resistant Tubes after 46,000 h Exposure to Reformer Service Conditions. *Metals*, *13*(2), Article 228. https://doi.org/10.3390/met13020228

metals

MDPI

Article

Failure Analysis of Two HP-Nb Heat-Resistant Tubes after 46,000 h Exposure to Reformer Service Conditions

Ali Nazemi Harandi [1,2,3], Abdoulmajid Eslami [1], Abbas Bahrami [1], Asghar Bakhtafrouz [3] and Maryam Yazdan Mehr [4,*]

[1] Department of Materials Engineering, Isfahan University of Technology, Isfahan 84156-83111, Iran
[2] Materials Engineering Group, Pardis College, Isfahan University of Technology, Isfahan 84156-83111, Iran
[3] Department of Research and Development, Rangin Zob Sepahan Company, Isfahan 84651-96973, Iran
[4] Faculty EEMCS, Delft University of Technology, Mekelweg 4, 2628 CD Delft, The Netherlands
* Correspondence: m.yazdanmehr@tudelft.nl

Abstract: This study presents a failure analysis in two reformer tubes used for hydrogen production in a petrochemical industry. These tubes (Tube A and Tube B) were made by the centrifugal casting of HP-Nb alloy in such a way that one contained titanium as a micro-element, and the other was free from titanium in its chemical composition. Although the two tubes were subjected to similar creep conditions, Tube A failed after only 46,000 h of operation against the design life of 100,000 h. SEM images showed initiation and growth of creep pores next to chromium carbide particles, as well as the formation of microcracks in $Cr_{23}C_6$ carbides. Pore initiation occurs as a result of grain boundary sliding and is strongly dependent on structural morphology. The tube containing titanium (Tube B) showed higher thermal stability and higher creep resistance than the tube without titanium (Tube A), which was due to the formation of finer and more discrete carbide particles. The final fracture of the tube without titanium (Tube A) occurred due to the coalescence of creep pores and the creation of grain boundary cracks.

Keywords: creep; failure analysis; HP-Nb heat-resistance steel; reformer tubes

Citation: Harandi, A.N.; Eslami, A.; Bahrami, A.; Bakhtafrouz, A.; Yazdan Mehr, M. Failure Analysis of Two HP-Nb Heat-Resistant Tubes after 46,000 h Exposure to Reformer Service Conditions. *Metals* **2023**, *13*, 228. https://doi.org/10.3390/met13020228

Academic Editor: George A. Pantazopoulos

Received: 20 December 2022
Revised: 19 January 2023
Accepted: 21 January 2023
Published: 26 January 2023

1. Introduction

HP steels are widely used for manufacturing heat-resistance tubes used in petrochemical plants. These tubes are often used in units to convert gases (a mixture of hydrocarbons) and water vapour into a hydrogen-rich gas or for other applications such as anomia or methanol production. During service, these tubes are exposed to quite high temperatures and relatively high internal pressures [1,2]. According to the API530 standard, these tubes are often designed to withstand a nominal life cycle of 100,000 h (11.4 years) [3]. The HP steel tubes are manufactured using centrifugal casting and modified with niobium offers excellent mechanical properties at high temperatures [4]. However, when these tubes are exposed to high temperatures and pressures, they often show cracks and premature failures compared to their normal life cycle as a result of creep or other failure mechanisms such as thermal fatigue, carburation, and oxidation [5–7].

The micro-structure of HP-Nb alloys mainly consists of an austenite matrix with complex carbide particles precipitated in the interdendritic spaces, while its morphology is highly dependent on the cooling rate during solidification. In fact, during the solidification of these tubes, elements such as Nb and Cr, as a result of saturation of austenite structure, are moved to the liquid phase before reacting with the free carbon and forming carbide particles in the interdendritic spaces [8]. The microstructure of these tubes, in the as-casted conditions, includes primary $M_{23}C_6$, M_7C_3, and MC carbides, which are precipitated in the boundary of austenite grains [9,10]. The microscopic structure of tubes changes significantly during service conditions and due to ageing. The full austenite matrix saturated with carbon creates a fine distribution of secondary carbides during service or ageing. Due to the role

of these precipitates as barriers to dislocation movements, this results in higher strength at higher temperatures. However, eventually, the coarsening of these strengthening particles results in an accelerated creep stage at high temperatures [10]. Furthermore, the formation of the G phase is another factor resulting in a decrease in creep resistance of these alloys [11]. In this regard, based on the findings by Yan et al. [12], the formation of the G phase decreases creep resistance in two ways. First, the conversion of niobium carbides to the G phase is accompanied by an increase in volume which results in stress and the formation of creep pores. Second, the formation of the G phase results in the formation of nickel-depleted zones in the surrounding regions, resulting in a decrease in creep resistance. Based on the failure analyses conducted by Min et al. [13], $M_{23}C_6$ precipitates and the G phase appear gradually at high temperatures and the coarsening of precipitates occurs next to grain boundaries. These changes in alloy morphology can result in the formation of creep pores or a decrease in creep resistance. According to the results presented by Andrade et al. [14], the failure mechanism of HP-Nb alloys changes from intragranular to grain boundary at temperatures higher than 1000 °C. This indicates a change in creep mechanism from slip-climb (dislocation creep) to atomic diffusion (grain boundary slip). There has been some research investigating the premature failure of HP reformer tubes. In this regard, Bahrami et al. [15] reported that reformer tubes have two types of grain structure: one is a dendrite structure initiating from the outer surface of the tube and continues until halfway into the tube's structure, while the other is a uniaxial structure initiating from the mid-way point and ending at the inner surface of the tube. The creep pores in the dendrite structure are formed next to dendrites and in the interdendritic spaces while the pores formed in the uniaxial zone have no specific direction or order and are distributed randomly inside the matrix. The creep pores are initiated on the surface of chromium and niobium carbides and their growth and coalescence result in crack formation. Fine carbide particles which result in higher creep resistance of these alloys are coarsened due to long exposure to high temperatures and create an ideal location for the initiation of creep pores. The separation and diffusion of alloying elements in the precipitate/matrix interface results in the formation of dealloyed regions which in turn results in the initiation and growth of pores and ultimately, brittle creep. Maharaj et al. [16] also investigated the failure mechanisms for HP reformers and reported that oxidation (or corrosion) plays an insignificant part in the failure due to the presence of creep pores and lack of oxygen at the crack's location, indicating that the crack has occurred solely formed due to creep. Furthermore, the higher temperature in certain areas closer to the burners had resulted in an increased creep failure rate in these areas. According to another study by Ma et al. [17], the thermal expansion coefficient of the austenite matrix is approximately twice that of chromium carbides. Therefore, at high temperatures the matrix expands more compared to carbide particles, applying stress to these particles and resulting in plastic deformation. Furthermore, carbides also impose compressive stresses within the matrix. This results in grain boundary slips which create creep pores in the matrix/carbide interface. The exposure to high temperatures also results in the formation of $Cr_{23}C_6$ precipitates and converts the niobium carbides to the G phase. The formation of secondary chromium carbides results in the formation of chromium-depleted regions in the surrounding areas. Furthermore, coarsening of grains and precipitates at high temperatures decreases the number of available diffusion paths from chromium-rich to chromium-depleted regions, making it more difficult to compensate for the chromium deficit in these regions. The presence of chromium-depleted regions decreases the alloy's strength and facilitates the formation of creep pores. On the other hand, the formation of the G phase in the place of niobium carbides results in a ductile phase replacing a hard phase, decreasing the overall strength of the alloy and facilitating the formation of creep pores. Kazempour et al. [18] reported that three zones were formed in the inner walls of the reformer tubes. The first zone (the inner-most zone) was an oxide layer, which itself consisted of two layers (a chromium oxide upper layer and a silicon oxide lower layer). The second zone was a carbon depleted zone which was rich in iron and nickel. Finally, the third zone

contained coarse interdendritic carbides and secondary carbides in an austenite matrix. The mentioned zones were also formed at the outer side of tube walls, with the difference that a thicker oxide layer was formed, while pores and cracks were also observed in the carbon-depleted zone. Pores were formed in the interface between carbides and austenite matrix. The pores were often isolated from one another and merged in one direction in certain areas. The cracks grew alongside the precipitates and chromium carbides undergo corrosion simultaneously.

In this study, the failure mechanism of HP-Nb centrifugal casting tubes after 46,000 h of service at the approximate temperature of 1000 °C in a petrochemical plant has been investigated. Failures in complicated systems often needs be addressed from different perspectives [19]. Lessons learned from such complicated failure conditions could benefit both industry and academia in dealing with these alloys.

2. Background and Failure Scenario

There was a failure in one section of centrifugal cast tubes in the reformer furnace, while other sections were sound. This caused attention, to do a RCFA on the subject. It turned out that the working conditions of the reformer tubes were almost similar, with some differences in the chemical composition of the failed part. In this regard, two heat-resistant tube sections after exposure to reformer service conditions were studied. Both tube sections were made of ASTM A 608 HP-Nb by centrifugal casting process, with the difference being that one was without Ti as the alloying element (Tube A), and the other was close to the failed section with Ti (Tube B). These tubes are welded together using the Gas Tungsten Arc Welding process before being placed in the reformer furnace. Both tune sections (Tube A and Tube B) were exposed to the same service conditions. Furnace feed, which includes desulphurised natural gas and water vapor, after reacting in the presence of nickel catalyst due to the combustion of furnace fuel, exits from the bottom of the furnace with a temperature of about 900 °C. The average external temperature of the tubes was 1000 °C and the relative pressure was 24.5 bar. In case of shut-downs, tubes are cooled down with the cooling rate of 60 °C per hour.

Figure 1a shows the location of these tube sections (Tube A and Tube B) in the reformer furnace. Although both tubes were under similar temperature and stress conditions, Tube A showed premature cracking and failure (Figure 1b). According to visual inspection, latitudinal cracks were observed at a distance of 6 mm from the welded joint in Tube A while no macroscopic cracks were observed in Tube B. The premature failure of the HP-Nb reformer tube without Ti (Tube A) after 46,000 h of service at the approximate temperature of 1000 °C as compared to Tube B (with 0.12% Ti) was studied. The observed damages included latitudinal cracks adjacent to the welding area, resulting in the need to replace the tubes after 46,000 h of service which is significantly lower than the expected life of the tubes.

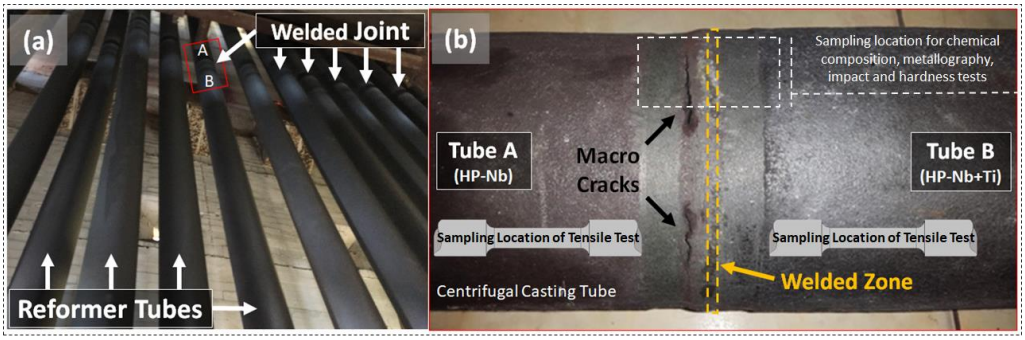

Figure 1. (**a**) Centrifugal cast tubes in the reformer furnace and (**b**) latitudinal cracks formed perpendicular to the stress direction on Tube A.

3. Materials and Methods

In this study, two aged tubes manufactured by centrifugal casting with an external diameter of 105 mm and a wall thickness of 11 mm were investigated. Both tubes were made from ASTM A 608 Grade HP-Nb, with slight differences in their composition such that Tube B also contained titanium as a microelement in its chemical composition (Table 1).

Table 1. The permitted range of various elements in the chemical composition of HP-Nb alloy along with the chemical composition of each tube, according to ASTM A 608-20 standard.

Sample	Grade	C	Ni	Cr	P	S	Si	Mn	Mo	Nb	Ti
ASTM A 608-20	HP-Nb	0.38–0.45	34.0–37.0	24.0–27.0	0.03 max	0.03 max	0.50–1.50	0.50–1.50	0.50 max	0.50–1.50	-
Tube A	HP-Nb	0.41	35.3	25.3	0.015	0.010	0.97	1.11	0.14	0.99	0.006
Tube B	HP-Nb+Ti	0.42	35.2	25.3	0.017	0.011	0.98	1.13	0.14	0.98	0.12

To investigate the cause of failure, samples were prepared from different cross-sections of the tubes for tensile strength, test impact test, hardness measurement, and chemical analysis (Figure 1b). Tensile test samples along the length of the tubes were prepared according to ASTM A370-21 standard and tensile properties were measured using Gotech AI 7000 LA-20 equipment (Gotech, Taichung Industry Park, Taichung City, Taiwan) with a strain rate of 5 mm/min. Macro hardness measurements were carried out using the Brinell method and ASTM E10-18 standard on the latitudinal cross-section of the samples. Impact tests were conducted using the Charpy method using the Gotech equipment model GT 7052-30 (Gotech, Taichung Industry Park, Taichung City, Taiwan).

Samples with dimensions of (10 × 10 × 10) mm^3 were prepared to investigate the microstructure in such a way as to include the welded zone and the base metal of the tubes. To check the microstructure in as-cast state, a sample was also prepared from the failed tube before being put into service condition. The samples were polished using sandpapers number 80 to 3000 before being polished with diamond paste with particle sizes of 0.3 and 0.05 micrometres in two steps. Micro etching of the samples was carried out using Marble's reagent for 25 s. Microstructural studies of the samples were conducted using a scanning electron microscope (SEM: Seron Technology, AIS-2100) (Serontech, Uiwang-si, Gyeonggi-do, Korea) equipped with point analysis EDS, EDAX, and BSE detector (and Philips, XL3, Eindhoven, The Netherlands).

4. Results and Discussion

The failed tube (tube A) showed several microstructural features. As can be seen in Figure 2a, the as-casted microstructure before exposure to service conditions consists of a primary carbide network (mostly including chromium and niobium carbides) in the interdendritic grain boundaries. Due to the low solubility of niobium in the austenite matrix, the niobium carbides precipitated at the grain boundaries or cell boundaries. This resulted in higher activation energy for slip and formation of creep pores, which can be supplied through stress or temperature [20]. Exposure of the tubes to high temperatures results in the conversion of the primary eutectic carbides to coarse $Cr_{32}C_6$ particles and the coalescence and precipitation of dispersed $Cr_{23}C_6$ carbides in the matrix (Figure 2b).

The high strength of the tubes at high temperatures is therefore based on the role of these precipitates as barriers for dislocation movement. On the other hand, coarsening of strengthening particles can result in a decrease of creep strength [10].

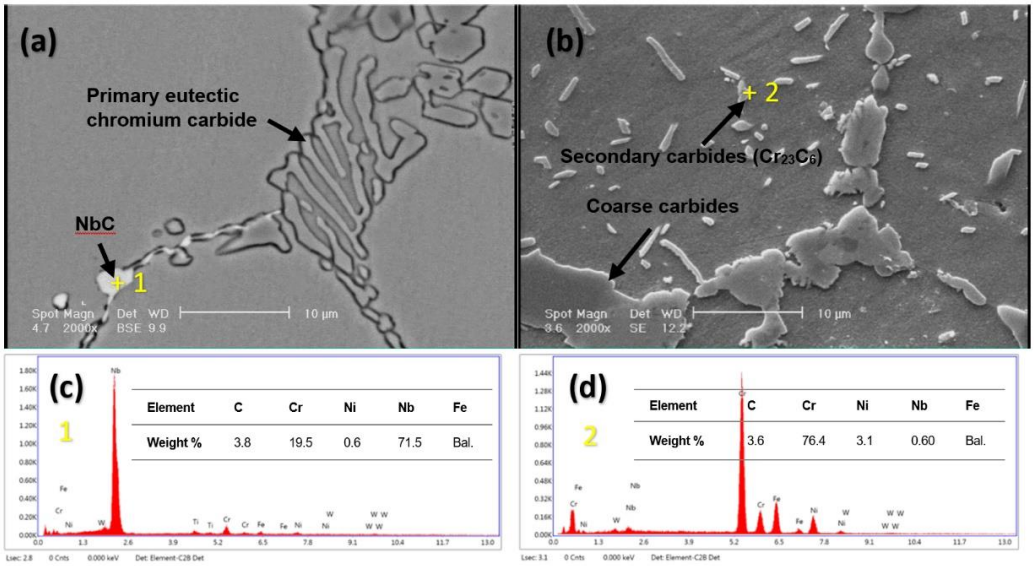

Figure 2. SEM images of Tube A (**a**) as-cased, and (**b**) after exposure to reformer service conditions for 46,000 h, (**c**,**d**) point elemental analysis of present phases using EDS system.

Near the outer shell of Tube A, a thin chromium-rich oxide layer and then a band of silicon oxides with an approximate thickness of 180 micrometres were observed (Figure 3a). In this region, despite the presence of niobium carbides as fine, dispersed particles (white precipitates), no chromium-rich precipitates were observed. The presence of the Cr_2O_3 layer has resulted in the depletion of chromium from adjacent areas in this layer, creating a region with no chromium-rich precipitates. Similarly, on the internal surface of the tube, oxide particles were observed at the boundary of austenite grains with an approximate thickness of 200 micrometres after the oxide layer (Figure 3b). These precipitates resulted in extreme brittleness of the tube and can be the initiation point for creep cracks. Carburation of the internal surface can automatically decrease the alloy's ductility at high temperatures. During this process, the formation of grain boundaries as microcrack sources results in decreased ductility. Furthermore, a decrease in chromium content in the matrix can result in the loss of oxide films on the internal surface of the tube, thus resulting in decreased corrosion resistance [21]. Although carburation and oxidation processes are known as the failure processes for reformer tubes, no sources for creep pores or cracks were observed next to the external or internal surface of the failed Tube A. In other words, the main reason for failure in Tube A is not the carburation of the internal surface or oxidation of the external surface of the tube.

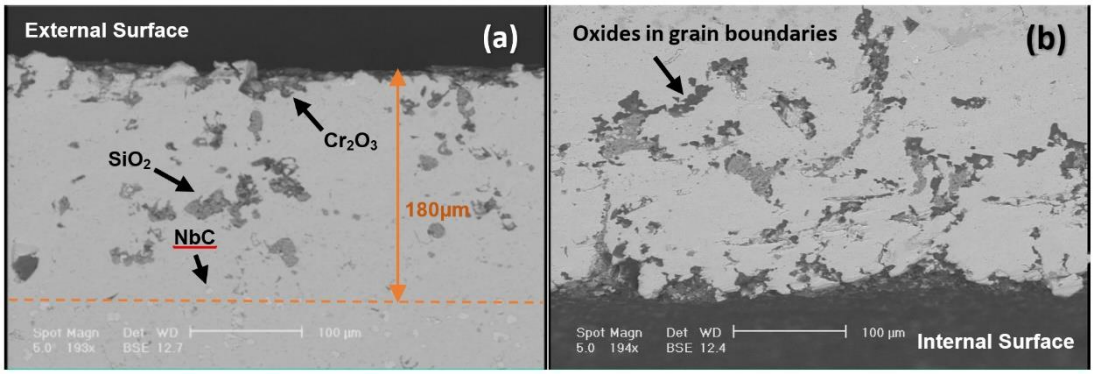

Figure 3. BSE micrograph of Tube A from (**a**) oxides and chrome-depleted zones near the external surface and (**b**) oxides and chrome-depleted zones near the internal surface of the tube.

Based on the results of atomic absorption spectroscopy analysis, the chemical composition in the analysed locations was within the boundaries specified in the ASTM A608 HP-Nb standard. Furthermore, the tube with higher resistance to failure (Tube B) contained a Ti microalloying element (Table 1). The addition of titanium results in finer and more refined precipitation in the inter-dendritic spaces during as-cast conditions and therefore delays the recovery mechanism through pinning of dislocations and grain boundaries [1]. Titanium changes the morphology of MC carbides from lamellar to blocky. Furthermore, complex niobium-titanium carbide (NbTiC) is formed and is more stable at higher temperatures. This increased stability of MC carbides controls their conversion to the G phase [22]. On the other hand, the transformation of niobium carbide into G phase removes the hard phase (NbC) which acts as a barrier against movement of dislocations, and therefore this transformation reduces the creep resistance [17]. According to the data presented by Zhang et al. [23], niobium-rich carbonitrides are dissolved in austenite at 1043 °C while titanium-rich carbonitrides are dissolved in austenite at 1406 °C. It is worth noting that the solid solution temperature (T_{AS}) has been calculated according to the following equations:

$$Log\ ([M]\ .\ [X]) = A - B/T \quad (1)$$

$$T_{\mathrm{AS}} = \frac{B}{A - log([M].[X])} \quad (2)$$

where A and B are constant values, and $[M]$ and $[X]$ are the mass fractions of elements in the austenite.

Our investigation showed that there is no evidence of the G phase in tubes containing titanium (Tube B). A low titanium concentration can result in the formation of niobium–titanium carbide complexes. Since titanium is insoluble in the G phase, it can increase the stability at higher temperatures and delay the transformation of (NbTi)C to the G phase. Therefore, the volume fraction of the G phase is lower in HP steel modified with Ti [22,24]. According to the X-Ray Mapping images presented in Figure 4, there are nickel, silicon, and niobium-rich areas identified in Tube A which is due to the presence of the G phase in tubes without titanium. These areas, indicated with arrows, have low chromium content, which, due to the lower strength and ductility of this phase compared to niobium carbides, are suitable areas for the initiation of creep pores. The volume expansion as a result of niobium carbide to G phase transformation can result in stress and therefore the formation of creep pores [12]. On the other hand, the transformation of niobium carbide into the G phase removes the hard phase (NbC) that can prevent the movement of dislocations and thus this phase transformation reduces the creep resistance [17].

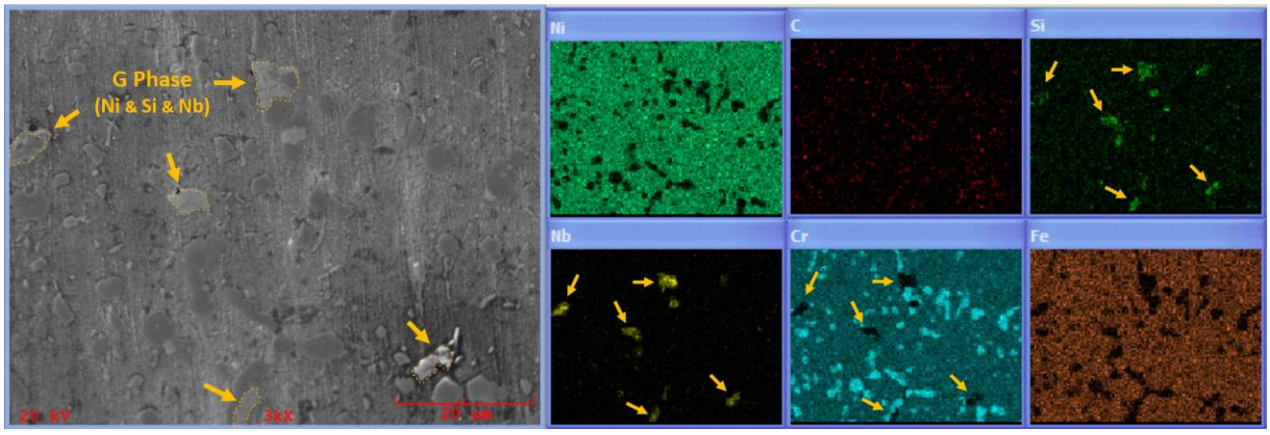

Figure 4. X-Ray Mapping images of tube A showing the distribution of various elements in SEM images.

According to Figure 5, the coalescence of the carbide network in the titanium-free sample is higher compared to the sample containing titanium. Furthermore, the tube

containing titanium as an alloying element (Tube B) has a finer structure. Therefore, based on the effects of microstructural morphology on the initiation, growth, and coalescence of creep pores, it is expected for the Tube B to have higher ductility and creep resistance compared to the Tube A. This improvement in creep behaviour can be due to the presence of Ti carbonitrides and their effect on secondary carbide precipitates during ageing. The reason for the lack of failure in Tube B, despite tolerating similar service conditions to Tube A, is the positive effects of titanium on the creep behaviour of the alloy.

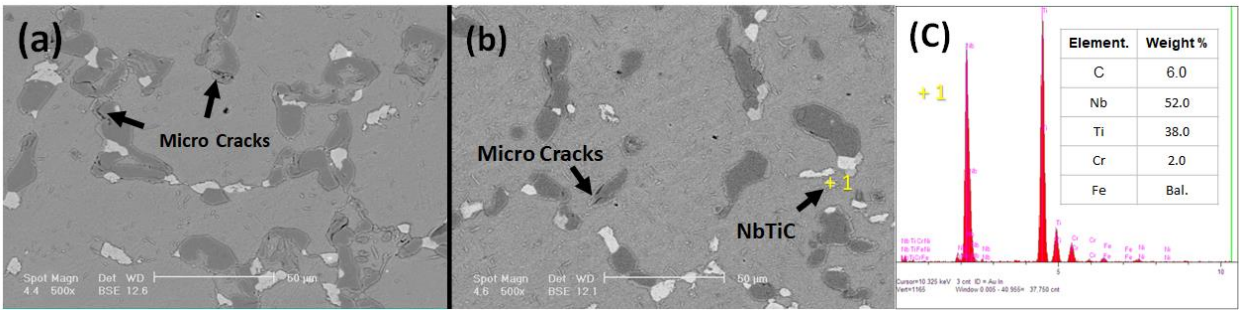

Figure 5. SEM images of tube microstructures after ageing: (**a**) Tube A without titanium and (**b**) Tube B containing 0.12 wt. % of titanium (**c**) point elemental analysis of NbTiC phase using EDS system.

Based on the impact and tensile strength test results, the lowest impact toughness strength and elongation values were observed for Tube A. The higher value of mechanical properties in Tube B as compared to Tube A is due to the effect of titanium on the microstructural morphology or separation between grain boundary carbides. The difference in the hardness values of the samples can be due to the presence of titanium-rich carbide particles in sample B (Table 2).

Table 2. The results of tensile strength, impact, and hardness tests.

Specimen	Elongation (%)	Yield Strength (N/mm^2)	Tensile Strength (N/mm^2)	Charpy Impact (J)	Hardness HB (2.5 × 62.5)
Tube A	1	184	253	8	235
Tube B	3	228	295	12	257

According to the data recorded during service conditions, the tubes have been exposed to 46 total unexpected furnace shutdowns. During unexpected shutdowns, the tubes are exposed to rapid cooling which undoubtedly results in thermal stress. During extreme service conditions, the thermo-mechanical strains can result in microstructural damages such as creep pores. The occurrence of these pores is not random but instead is related to some of the microstructural properties of the materials. As a result, almost all creep pores are formed next to carbide particles or in the carbide-austenite interfaces. The aged reformer tubes are more sensitive to thermal shocks due to their more brittle nature. As can be seen in Figure 6, the effect of thermal stress has resulted in the formation of microcracks on the chromium carbide particles.

According to the SEM images obtained from the microstructure of failed tube (Tube A) close to the main crack, the creep pores have initiated on grain boundaries perpendicular to the direction of the applied stress and their number and size has increased over time. The continuous initiation of creep pores in this case is dependent on the strain and is generally facilitated by the cracks formed on the $Cr_{23}C_6$ carbide particles. As shown in Figure 7a,b, intergranular fracture occurred along the continuous carbides, and creep voids grew more on coarser carbides, especially in the triple grain boundary regions. According to spot analysis (Figure 7c) and the weight ratio of carbon and chromium, the stoichiometry of these carbides is mainly $Cr_{23}C_6$.

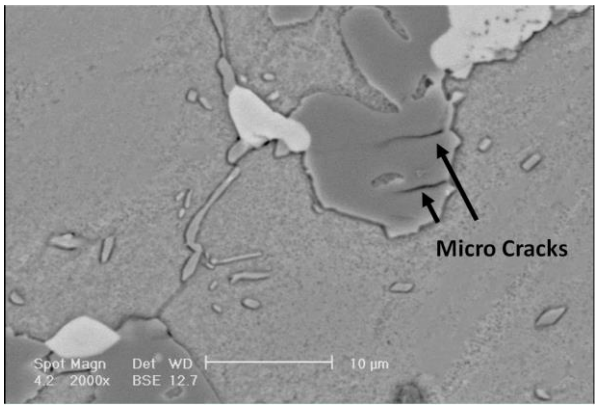

Figure 6. SEM images of microstructure of failed tube (Tube A). Micro cracks formed within chromium carbide particles are indicated with the arrows.

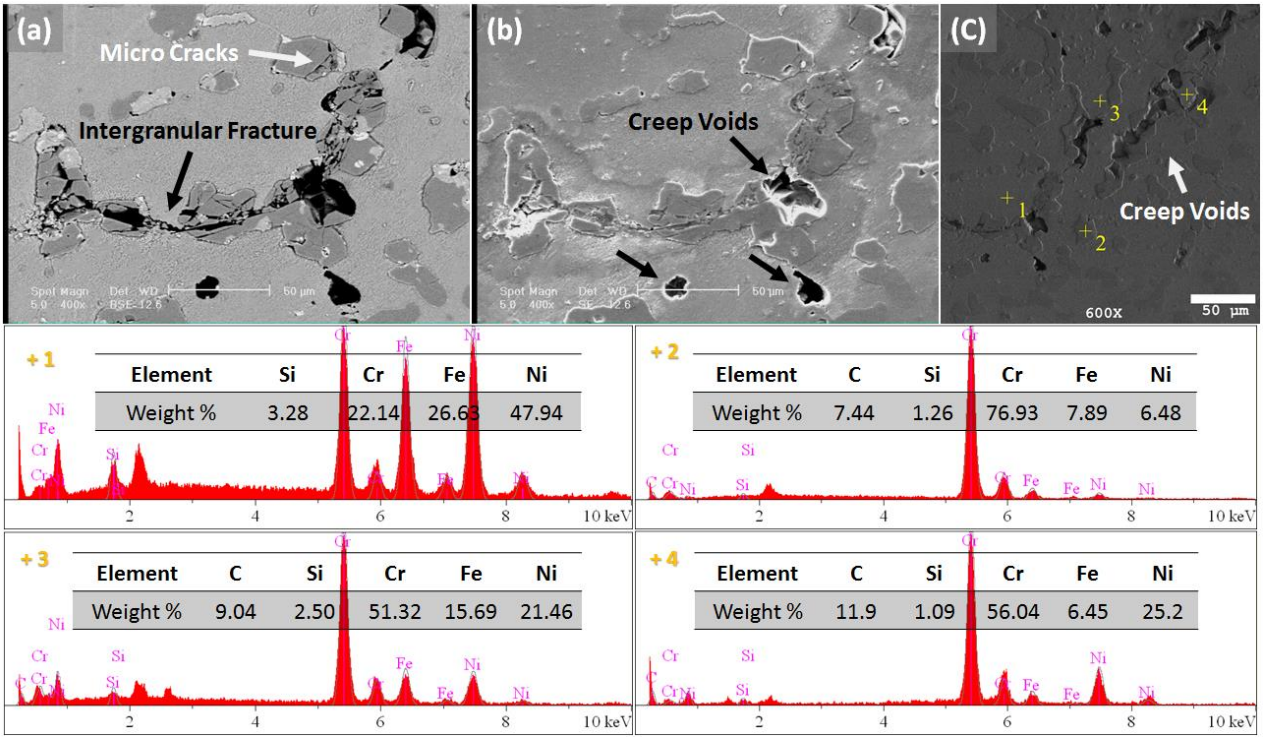

Figure 7. (**a**,**b**) SEM images of Microstructure degradation of Tube A, (**c**) point analysis of phases in the degraded area using SEM equipped with an EDS. The growth of creep voids and propagation of microcracks at grain boundaries and chromium carbides are shown.

The SEM studies of the interface between the welded area and base metal in Tube A show no evidence of creep pores or microcracks in the welded zone. However, creep pores and microcracks are apparent at approximately 200 microns from the welded line in the base metal of Tube A (Figure 8a). This can be due to the presence of larger carbide particles in the base metal compared to the welded zone. As shown in Figure 8b, small and individual creep voids have nucleated in a base metal of the Tube B, but they have not been able to grow. This issue can be caused by the difference in microstructural morphology between Tube A and Tube B in terms of the distribution and size of chromium carbides.

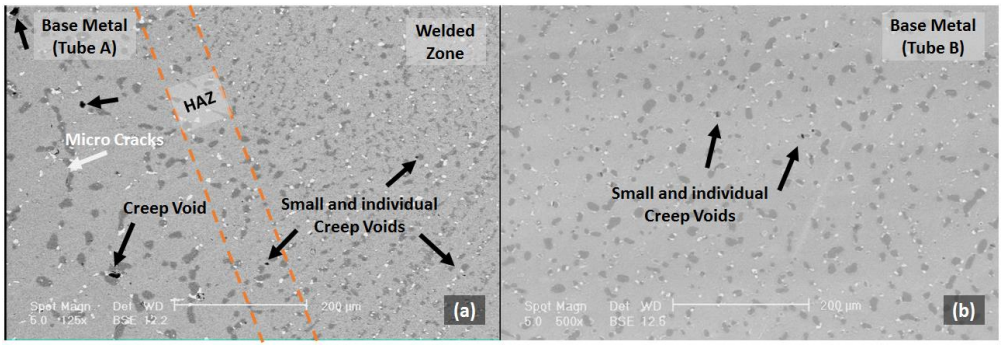

Figure 8. SEM images of (**a**) the interface between welded zone and base metal in tube A, (**b**) base metal in tube B.

The decrease in the life cycle of reformer tubes is determined under the influence of creep damage which is indicated by progressive changes in the microstructure. The transfer of carbides, initiation of microcracks, and formation of creep pores often occur in the final stage of the creep damage and immediately before the failure. The growth of these creep pores mostly occurs perpendicular to the direction of the applied stress, and their growth rate is controlled by localized creep strain. The final fracture occurs due to pile-up of the pores, formation of grain boundary cracks, and an increase in the number and size of cracks. According to Figure 9, creep cavities are mostly observed in the triple or wedge-shaped areas and on chromium carbide particles. Coarsened chromium carbide particles merge under the influence of reformer temperature, and create suitable areas for initiation of creep pores. The pile-up of grain boundary cracks also occurs along the length of chromium carbide particles, indicating merged carbide particles as preferred crack initiation zones.

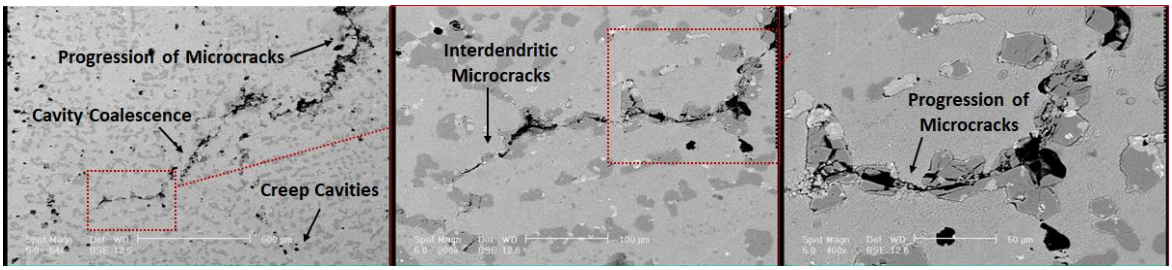

Figure 9. SEM images showing the pile-up of creep pores along the length of grain boundaries or inside grain boundary carbide particles and coalescence for the formation of cracks in the failed tube.

Based on the results of fractography studies, the fracture morphology of the failed tube (Tube A) is jagged, which indicates unsuitable mechanical properties. The furrow and ridges distributed on the fracture surface are seen in Figure 10a. The porosity has resulted in non-uniformity of distribution in tensile/compression stress. The imaginary line indicates the boundary between ductile and brittle fracture zones. As can be seen in Figure 10b, the fracture is ductile using the void coalescence mechanism in the areas with merged carbide particles (arrows). These microvoids are a suitable location for the coalescence of cracks due to the increase in local stress.

Exposure to high temperatures results in the dissolution of carbide particles present in the structure. This removes the barriers to dislocation movements and decreases creep strength. These conditions lead to the formation of creep pores perpendicular to the direction of the applied stress. Over time, these pores coalesce together and create microcracks. Finally, the growth of microcracks results in the formation of macrocracks and the failure of the specimen. The failure scenario is schematically shown in Figure 11 and summarized in the following steps: including initiation of isolated cavities, aligned cavities, and the formation of microcracks next to continuous carbide particles.

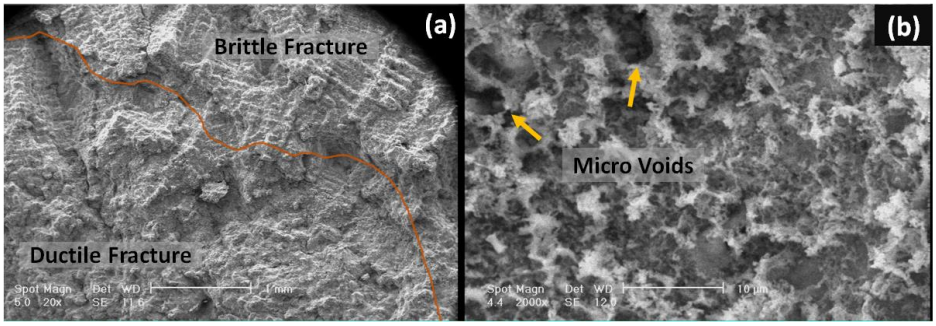

Figure 10. SEM images of fracture surface morphology of the failed tube, (**a**) final ductile and brittle fracture surfaces and (**b**) ductile fracture surface.

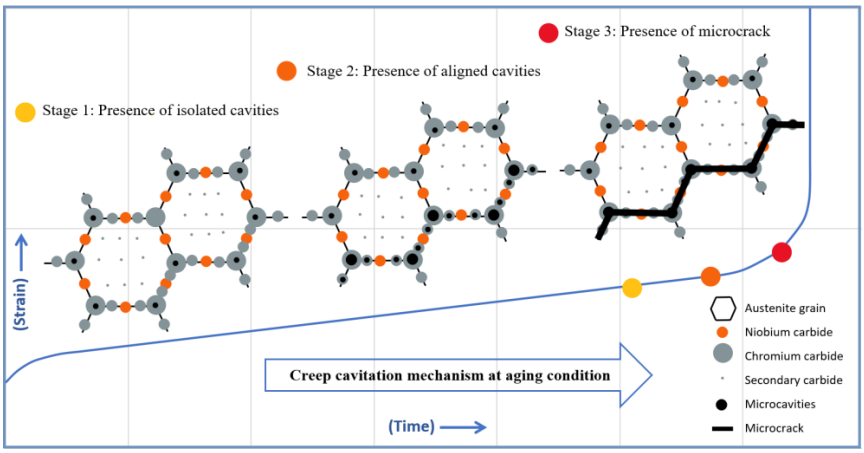

Figure 11. The initiation and growth mechanism for creep pores adjacent to interdendritic carbide particles during service transposed on a general creep graph.

As a result of cyclic mechanical and thermal loadings caused by unexpected shut-downs, the thermal-mechanical fatigue process leads to microstructural damages such as carbide cracks and creep pores. According to Figure 12, the macrocracks are formed as a result of the coalescence of microcracks formed on the surface of chromium carbide particles as well as creep pores. The growth rate of these cracks is proportional to the applied strain and these cracks are grown perpendicular to the direction of applied stress. The creep behaviour of studied tubes in the current study is highly dependent on the difference in microstructural properties as a result of the addition of titanium to HP-Nb alloy.

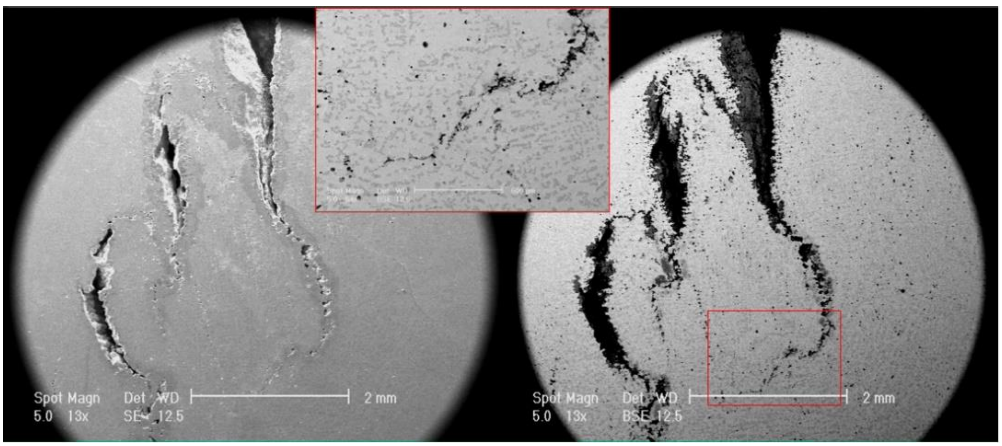

Figure 12. SEM images of cracked regions; directional creep pores are seen along the length of main cracks. The singular creep pores have a uniform distribution in the matrix.

5. Conclusions

- It was shown that after 46,000 h at temperature of 1000 °C the microstructure of Tube A is generally subjected to degradation: coalescence and coarsening of carbides, nucleation of creep voids, voids coalescence, interdendritic microcracks, and final propagation of macrocracks. The fracture mechanism is intergranular, especially when creep voids on coalescence carbides can grow.
- Long exposure of the tubes to the reformer service conditions and unexpected shutdowns during service conditions and the resulting rapid cooling create thermal stress in reformer tubes and lead to the formation of creep cracks, resulting in microstructural changes, including coarsening and formation of blocky primary eutectic carbide particles, formation of microcracks, and the initiation of creep pores on the austenite grain boundaries and chromium carbide particles. Thus, an increase in the tubes' sensitivity to thermal stresses was caused by unexpected shutdowns, and is eventually decreasing in designed creep life.
- The presence of titanium in the chemical composition of Tube B resulted in the formation of fine and discontinuous precipitates, thus increasing in the ductility during creep service conditions. On the other hand, titanium formed complex carbide compounds along with niobium, which mostly prevented the decomposition of niobium carbides and the formation of the undesirable G phase. Furthermore, due to the higher dissolution temperature for titanium carbides compared to chromium and niobium carbides, the precipitates were more resistant to high temperatures. Overall, the mentioned factors increased the creep strength of Tube A, containing titanium as a micro-element additive.

Author Contributions: A.N.H.: Data curation; Formal analysis; Investigation; Writing, A.E.: Supervision; Methodology. A.B. (Abbas Bahrami): Supervision; Methodology, Writing—review and editing, A.B. (Asghar Bakhtafrouz): Supervision; Methodology. M.Y.M.: Supervision; Writing—review and editing; Investigation. All authors have read and agreed to the published version of the manuscript.

Funding: This research received no external funding.

Institutional Review Board Statement: Not applicable.

Informed Consent Statement: Not applicable.

Data Availability Statement: Not applicable.

Acknowledgments: The authors wish to offer their thanks and appreciation to Isfahan University of Technology, Rangin Zob Sepahan Co. and Delft University of Technology for their support and involvement during this study.

Conflicts of Interest: The authors declare no conflict of interest.

References

1. Garbiak, M.; Jasiński, W.; Piekarski, B. Materials for Reformer Furnace Tubes. History of Evolution. *Arch. Foundry Eng.* **2011**, *11*, 47–52.
2. Bhaumik, S.K.; Rangaraju, R.; Parameswara, M.A.; Bhaskaran, T.A.; Venkataswamy, M.A.; Raghuram, A.C.; Krishnan, R.V. Failure of Reformer Tube of an Ammonia Plant. *Eng. Fail. Anal.* **2002**, *9*, 553–561. [CrossRef]
3. *Standard A.P.I. 530*; Calculation of Heater-Tube Thickness in Petroleum Refineries. American Petroleum Institute: Washington, DC, USA, 2015.
4. Taghipour, M.; Eslami, A.; Bahrami, A. High Temperature Oxidation Behavior of Aluminide Coatings Applied on HP-MA Heat Resistant Steel Using a Gas-Phase Aluminizing Process. *Surf. Coat. Technol.* **2022**, *434*, 128181. [CrossRef]
5. Xia, Y.; Shi, M.; Zhang, C.; Wang, C.; Sang, X.; Liu, R.; Zhao, P.; An, G.; Fang, H. Analysis of flexural failure mechanism of ultraviolet cured-in-place-pipe materials for buried pipelines rehabilitation based on curing temperature monitoring. *Eng. Fail. Anal.* **2022**, *142*, 106763. [CrossRef]
6. Roy, N.; Raj, A.; Roy, B.N.; Ray, A.K. Creep Deformation and Damage Evaluation of Service Exposed Reformer Tube. *Can. Metall. Q.* **2015**, *54*, 205–222. [CrossRef]
7. Pourmohammad, H.; Bahrami, A.; Eslami, A.; Taghipour, M. Failure Investigation on a Radiant Tube in an Ethylene Cracking Unit. *Eng. Fail. Anal.* **2019**, *104*, 216–226. [CrossRef]

8. Andrade, A.R.; Bolfarini, C.; Ferreira, L.A.M.; Vilar, A.A.A.; Souza Filho, C.D.; Bonazzi, L.H.C. Influence of Niobium Addition on the High Temperature Mechanical Properties of a Centrifugally Cast HP Alloy. *Mater. Sci. Eng. A* **2015**, *628*, 176–180. [CrossRef]
9. Taghipour, M.; Eslami, A.; Salehi, M.; Bahrami, A. An Investigation on Anti-Coking Behavior of Gas Phase Aluminide Coatings Applied on a High Performance Micro Alloyed (HP-MA) Steel. *Surf. Coat. Technol.* **2020**, *389*, 125607. [CrossRef]
10. Nunes, F.C.; De Almeida, L.H.; Dille, J.; Delplancke, J.-L.; Le May, I. Microstructural Changes Caused by Yttrium Addition to NbTi-Modified Centrifugally Cast HP-Type Stainless Steels. *Mater. Charact.* **2007**, *58*, 132–142. [CrossRef]
11. Alvino, A.; Ramires, D.; Tonti, A.; Lega, D. Influence of Chemical Composition on Microstructure and Phase Evolution of Two HP Heat Resistant Stainless Steels after Long Term Plant-Service Aging. *Mater. High Temp.* **2014**, *31*, 2–11. [CrossRef]
12. Yan, J.; Gao, Y.; Yang, F.; Yao, C.; Ye, Z.; Yi, D.; Ma, S. Effect of Tungsten on the Microstructure Evolution and Mechanical Properties of Yttrium Modified HP40Nb Alloy. *Mater. Sci. Eng. A* **2011**, *529*, 361–369. [CrossRef]
13. Yu, J.M.; Dao, V.H.; Lok, V.; Le, T.G.; Yoon, K.B. Asymptotic Creep Deformation Behavior of Modified HP Steel after Long-Term Service. *J. Mech. Sci. Technol.* **2020**, *34*, 1997–2009. [CrossRef]
14. Andrade, A.R.; Bolfarini, C.; Ferreira, L.A.M.; Souza Filho, C.D.; Bonazzi, L.H.C. Titanium Micro Addition in a Centrifugally Cast HPNb Alloy: High Temperature Mechanical Properties. *Mater. Sci. Eng. A* **2015**, *636*, 48–52. [CrossRef]
15. Bahrami, A.; Taheri, P. Creep Failure of Reformer Tubes in a Petrochemical Plant. *Metals* **2019**, *9*, 1026. [CrossRef]
16. Maharaj, C.; Marquez, A.; Khan, R. Failure Analysis of Incoloy 800HT and HP-Modified Alloy Materials in a Reformer. *J. Fail. Anal. Prev.* **2019**, *19*, 291–300.
17. Ma, Y.W.; Yang, G.; Yoon, K.B.; Le, T.G. Microstructure Evaluation During Short Term Creep of Cr35Ni45Nb Cast Alloy Reformer Tube. *Met. Mater. Int.* **2021**, *27*, 5165–5172. [CrossRef]
18. Kazempour-Liasi, H.; Lalegani, Z.; Rayatpour, M. Life Assessment of HP-40Nb Reformer Furnace Tube of a Petrochemical Plant. *Strength Mater.* **2021**, *53*, 364–375. [CrossRef]
19. Zhang, P.; Liu, Z.; Yue, X.; Wang, P.; Zhai, Y. Water jet impact damage mechanism and dynamic penetration energy absorption of 2A12 aluminum alloy. *Vacuum* **2022**, *206*, 111532. [CrossRef]
20. Kirchheiner, R.; Woelpert, P. Niobium in Centrifugally Cast Tubes for Petrochemical Applications. In Proceedings of the International Symposium Niobium, Orlando, FL, USA, 2–5 December 2001.
21. McLeod, A.C.; Bishop, C.M.; Stevens, K.J.; Kral, M. V Microstructure and Carburization Detection in HP Alloy Pyrolysis Tubes. *Metallogr. Microstruct. Anal.* **2015**, *4*, 273–285. [CrossRef]
22. De Almeida, L.H.; Ribeiro, A.F.; Le May, I. Microstructural Characterization of Modified 25Cr–35Ni Centrifugally Cast Steel Furnace Tubes. *Mater. Charact.* **2002**, *49*, 219–229. [CrossRef]
23. Zhang, Y.; Li, X.; Liu, Y.; Liu, C.; Dong, J.; Yu, L.; Li, H. Study of the Kinetics of Austenite Grain Growth by Dynamic Ti-Rich and Nb-Rich Carbonitride Dissolution in HSLA Steel: In-Situ Observation and Modeling. *Mater. Charact.* **2020**, *169*, 110612. [CrossRef]
24. Piekarski, B. Effect of Nb and Ti Additions on Microstructure, and Identification of Precipitates in Stabilized Ni-Cr Cast Austenitic Steels. *Mater. Charact.* **2001**, *47*, 181–186. [CrossRef]